



Synthesis and characterization of electrospun molybdenum dioxide–carbon nanofibers as sulfur matrix additives for rechargeable lithium–sulfur battery applications

Ruiyuan Zhuang^{‡1}, Shanshan Yao^{*‡1}, Maoxiang Jing¹, Xiangqian Shen^{1,2}, Jun Xiang³, Tianbao Li², Kesong Xiao² and Shibiao Qin²

Full Research Paper

[Open Access](#)

Address:

¹Institute for Advanced Materials, College of Materials Science and Engineering, Jiangsu University, Zhenjiang, 212013, P. R. China, ²Hunan Engineering Laboratory of Power Battery Cathode Materials, Changsha Research Institute of Mining and Metallurgy, Changsha, 412212, P. R. China and ³School of Mathematics and Physics, Jiangsu University of Science and Technology, Zhenjiang, 212013, P. R. China

Email:

Shanshan Yao^{*} - yaosshan@ujs.edu.cn

* Corresponding author ‡ Equal contributors

Keywords:

electrochemical performance; electrospinning; lithium–sulfur batteries; MoO₂–CNFs; sulfur matrix

Beilstein J. Nanotechnol. **2018**, *9*, 262–270.

doi:10.3762/bjnano.9.28

Received: 29 July 2017

Accepted: 25 December 2017

Published: 24 January 2018

Associate Editor: N. Motta

© 2018 Zhuang et al.; licensee Beilstein-Institut.

License and terms: see end of document.

Abstract

One-dimensional molybdenum dioxide–carbon nanofibers (MoO₂–CNFs) were prepared using an electrospinning technique followed by calcination, using sol–gel precursors and polyacrylonitrile (PAN) as a processing aid. The resulting samples were characterized by X-ray diffraction (XRD), Fourier transform infrared spectroscopy (FTIR), Raman spectroscopy, Brunauer–Emmet–Teller (BET) surface area measurements, scanning electron microscopy (SEM) and transmission electron microscopy (TEM). MoO₂–CNFs with an average diameter of 425–575 nm obtained after heat treatment were used as a matrix to prepare sulfur/MoO₂–CNF cathodes for lithium–sulfur (Li–S) batteries. The polysulfide adsorption and electrochemical performance tests demonstrated that MoO₂–CNFs did not only act as polysulfide reservoirs to alleviate the shuttle effect, but also improve the electrochemical reaction kinetics during the charge–discharge processes. The effect of MoO₂–CNF heat treatment on the cycle performance of sulfur/MoO₂–CNFs electrodes was examined, and the data showed that MoO₂–CNFs calcined at 850 °C delivered optimal performance with an initial capacity of 1095 mAh g^{−1} and 860 mAh g^{−1} after 50 cycles. The results demonstrated that sulfur/MoO₂–CNF composites display a remarkably high lithium–ion diffusion coefficient, low interfacial resistance and much better electrochemical performance than pristine sulfur cathodes.

Introduction

Lithium–sulfur (Li–S) batteries are considered to be the most promising candidates for the next green rechargeable batteries due to their high energy density (2600 Wh kg^{-1}) and theoretical specific capacity (1675 mAh g^{-1}). However, before Li–S batteries become a viable technology, some challenges need to be solved such as the insulating nature of sulfur and the shuttle effect caused by dissolved polysulfide molecules [1]. All of these issues still pose a challenge to overcome for the production of reversible, stable, and efficient sulfur cathodes. The currently proposed approaches to solve these issues include sulfur-based cathode modification, electrolyte modification and new cell configuration [2].

Overall, it is critical to enhance the utilization of sulfur and stabilize the polysulfide within the cathodic region to yield Li–S batteries with improved electrochemical performance. For the past two decades, various carbon materials (e.g., mesoporous carbon [3], multiwalled carbon nanotubes (MWNTs) [4] and hollow carbon microspheres [5]) and electrically conductive polymeric materials (e.g., polyaniline [6], polypyrrole [7] and poly(3,4-ethylenedioxythiophene) [8]) have been considerably used to encapsulate sulfur or polysulfide. Recently, polar metal oxide/sulfide materials including SiO_2 [9], TiO_2 [10], MnO_2 [11], $\text{Mg}_{0.6}\text{Ni}_{0.4}\text{O}$ [12], TiS_2 [13], CoS_2 [14], and FeS_2 [15] were found to be more highly effective in binding with sulfur species than carbon substrates, and were found to significantly improve the cycling behavior of Li–S batteries. However, these metal oxide/sulfide materials have low electrical conductivity, which makes the chemically adsorbing polysulfides difficult to be reduced directly on the matrix surface, resulting in the lower reutilization of the active sulfur material. In order to improve the kinetics of the electrode redox reaction, the electrical conductivity of Ti_4O_7 nanoparticles [16,17] and Co_9S_8 [18] nanosheets have been used in new concepts for sulfur matrices with both a polar nature and good conductivity. Therefore, the exploration of novel conductive composites is another direction leading to the practical application of Li–S batteries.

Molybdenum dioxide (MoO_2) materials are particularly attractive among the transition-metal oxides due to their high melting point, high chemical stability and low electrical resistivity (190 S cm^{-1}). This material has great potential for applications in several fields such as sensing, catalysis, supercapacitors and as an anode material in lithium ion batteries due to its relatively large theoretical capacity [19–21]. Although numerous synthetic approaches have been reported for preparing MoO_2 nanostructures with diverse morphologies, the fabrication, manipulation, and engineering of one-dimensional (1D) MoO_2 -CNFs nanocomposites, especially with secondary MoO_2 nanostructures, are difficult to achieve due to lack of appropriate and

generalized synthetic methodologies. Recently, hierarchical MoO_2/C microspheres and hierarchical $\text{MoO}_2/\text{Mo}_2\text{C}/\text{C}$ hybrid nanowires were fabricated using organic–inorganic precursors and self-templates, which were used as anode materials in lithium ion batteries [22,23]. However, since electrospinning is a simple and versatile method for producing fibers from a variety of materials on a large scale, it has attracted much attention in both research and commerce [24]. The nanofibers have extremely high specific surface area because of their small diameter and their porosity which exhibits excellent pore interconnectivity [25,26]. To the best of our knowledge, no articles related to using MoO_2 -CNFs as a sulfur matrix in Li–S batteries have been published so far.

In the present work, a facile route based on a single-spinneret electrospinning technique with a subsequent annealing process was developed to prepare MoO_2 -CNFs. The effect of MoO_2 -CNF heat treatment on the cycle performance of sulfur/ MoO_2 -CNFs electrodes was examined. The data showed that MoO_2 -CNFs calcined at $850 \text{ }^\circ\text{C}$ delivered optimal performance, with an initial capacity of 1095 mAh g^{-1} and retained a capacity of 860 mAh g^{-1} after 50 cycles. The results demonstrated that the sulfur/ MoO_2 -CNF composite displays a markedly high lithium-ion diffusion coefficient, a low interfacial resistance and much better electrochemical performance than a pristine sulfur cathode.

Results and Discussion

Characterization of MoO_2 -CNFs

X-ray diffraction (XRD) patterns of the as-prepared composite fibers calcined at various temperatures are presented in Figure 1a. Well-defined features appeared for the samples heated at $550 \text{ }^\circ\text{C}$ due to the crystallization of MoO_2 . Five main peaks at 2θ of 25.8° , 36.8° , 53.4° , 60.4° and 66.7° were assigned to the crystallographic planes of (011), (200), (220), (310) and (202), respectively. These corresponded to pure phase MoO_2 with monoclinic symmetry, which agreed well with the JCPDS card of MoO_2 (78-1072). As the calcination temperature was raised to $850 \text{ }^\circ\text{C}$, the characteristic diffraction peaks of MoO_2 became sharper and displayed higher intensities, indicating an increase in the crystallinity of MoO_2 as shown in Table 1. Meanwhile, this was also reflected in the surface area, which decreased as the calcination temperature increased (Table 1).

The lattice parameters of the as-prepared MoO_2 nanoparticles are listed in Table 2. The lattice parameters of the MoO_2 phase decreased as the calcination temperature increased, which also reflects the change produced by the varying size of the MoO_2 nanoparticles. At the calcination temperature of $900 \text{ }^\circ\text{C}$, the pri-

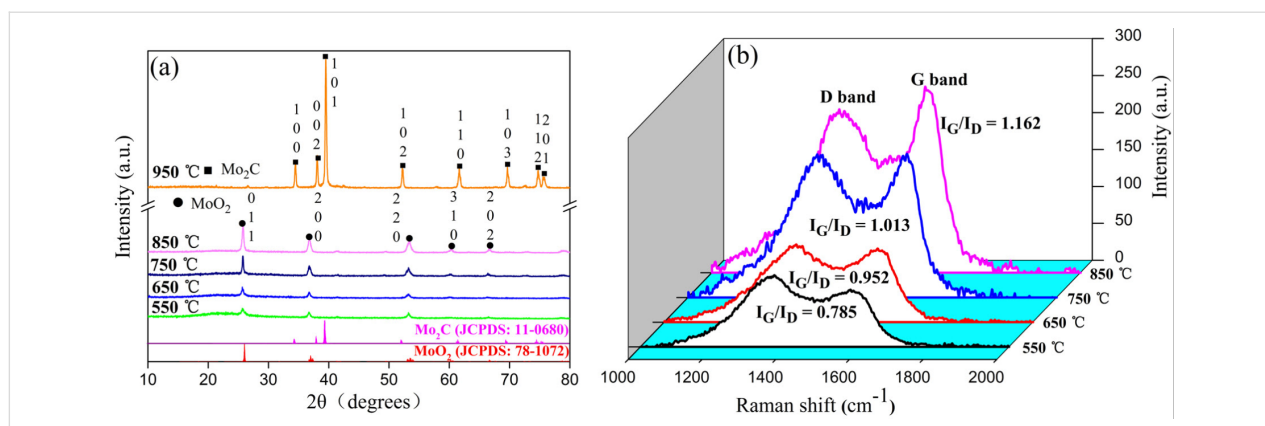


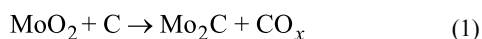
Figure 1: (a) XRD pattern and (b) Raman spectra of the MoO₂-CNFs calcined at various temperatures.

Table 1: Effect of calcination temperature on BET surface area and particle size of MoO₂.

Calcination temperature (°C)	BET surface area (m ² g ⁻¹)	Particle size (nm) ^a
550	312.65	42.93
650	226.30	50.67
750	182.33	58.48
850	142.69	68.24

^aCalculated using the Scherrer equation.

mary phase of the sample became Mo₂C, but small diffraction peaks of MoO₂ could be identified. After calcination at 950 °C, the MoO₂ nanoparticles reacted with carbon during the carbonation process to form Mo₂C, according to Equation 1:



Mo₂C is known to be active in numerous reactions associated with noble metals, such as CO₂ hydrogenation, water gas shift, alcohol synthesis and hydrazine decomposition. Here, CH₄/H₂ atmosphere was not used during calcination, which was much safer and facile when compared to other methods [27].

Table 2: Effect of calcination temperature on BET surface area and particle size of MoO₂.

Sample	<i>a</i> (Å)	<i>b</i> (Å)	<i>V</i> (Å ³)
MoO ₂ -CNF (550 °C)	5.6512	4.8633	132.9862
MoO ₂ -CNF (650 °C)	5.6343	4.8602	132.1328
MoO ₂ -CNF (750 °C)	5.6203	4.8573	131.9487
MoO ₂ -CNF (850 °C)	5.6128	4.8535	131.8365
MoO ₂ (JCPDS:78-1072)	5.6500	4.8600	132.9500

Raman spectroscopy is a very useful tool for the characterization of carbon-based nanostructures. The Raman spectra

of the products excited with a 532 nm laser line are shown in Figure 1b. Two characteristic peaks at around 1355 and 1580 cm⁻¹ correspond to disordered carbon (D-band) and graphite carbon (G-band), respectively. Integrating of the areas of the D and G peaks yielded a significant enhancement in the corresponding *I*_G/*I*_D ratio. Thus, it could be concluded that an increased calcination temperature led to the formation of significant amounts of graphitic carbon. Both the XRD and Raman spectra revealed that MoO₂-CNF was successfully prepared through electrospinning.

The Fourier transform infrared spectroscopy (FTIR) spectra of PAN fibers, as-prepared composite PAN/PMA fibers, and composite fibers calcined at different temperatures are illustrated in Figure 2. The FTIR spectra of PAN fibers and as-prepared PAN/PMA fibers presented characteristic absorption peaks at 2242 cm⁻¹ (C≡N) and 1736 cm⁻¹ (C=O), indicating that PAN

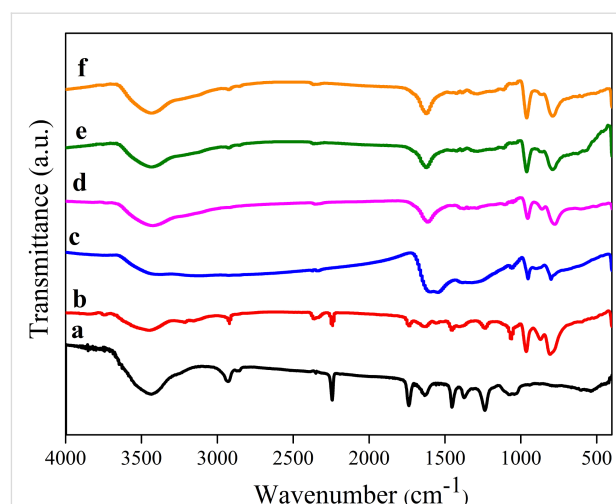


Figure 2: FTIR spectra of (a) PAN fibers and MoO₂-CNFs (b) as-prepared PAN/PMA composite fibers, and (c-f) fibers calcined at 550 °C, 650 °C, 750 °C and 850 °C, respectively.

played the role of a copolymer or that the DMF solvents did not entirely volatilize (Figure 2a,b). The bands in the regions of 2934–2890, 1465–1445, 1385–1355, and 1270–1210 cm^{-1} were assigned to the aliphatic CH group vibrations of different modes in CH, CH_2 and CH_3 . After calcination from 550 °C to 850 °C, the absorption bands of PAN vanished due to decomposition and removal of the organic groups. The peak at 925 cm^{-1} was associated with Mo=O, while the prominent bands in the range of 500–850 cm^{-1} were attributed to Mo–O–Mo, indicating the occurrence of crystallization [28]. Both the Raman spectra and XRD results suggested that MoO_2 -CNFs were formed through a subsequent annealing process. The broad band at 3400 cm^{-1} was attributed to the O–H stretching vibration due to adsorbed H_2O molecules on the nanofibers of KBr.

A photo of the nonwoven PAN/PMA material is depicted in Figure 3a. The morphology of the as-prepared composite fibers and calcined fibers was further characterized by FE-SEM and TEM. The PAN/PMA composite fibers showed smooth surfaces due to their amorphous nature (Figure 3b). The average diameter of the as-prepared composite fibers was estimated to be 485 nm. After calcination of the fibers at 550 °C, the surface became rough and the average diameter decreased to 425 nm.

The shrinkage and reduction in the fibers was caused by decomposition of PAN and subsequent crystallization. After calcination at 650 °C and 750 °C, MoO_2 -CNFs showed discrete lengths with average diameters of 506 nm and 575 nm, respectively. Also, the diameter of MoO_2 -CNF increased as the calcination temperature was increased, which can be explained by the gradual increase in grain size of MoO_2 with sintering temperature. Interestingly, a change in fiber morphology was observed when the calcination temperature increased to 850 °C. The nanofibers consisted of connected particles or crystallites, which is consistent with previous reports [29]. Further structural characterization of the as-prepared MoO_2 -CNFs was performed by TEM. Figure 3g shows a typical TEM photograph of the nanostructures, displaying MoO_2 nanoparticles decorated with carbon nanofibers. The elemental EDX of MoO_2 -CNFs depicted in Figure 3h indicates the presence of elemental Mo, O, C and Cu. The Cu signal comes from the Cu grid. The HRTEM image indicated that the grown structure was single crystalline with a lattice spacing of 0.344 nm, corresponding to the [11] crystal plane of monoclinic MoO_2 (Figure 3i).

SEM images of pure sulfur and S/ MoO_2 -CNF composites are displayed in Figure 4a,b, respectively. The sulfur morphology

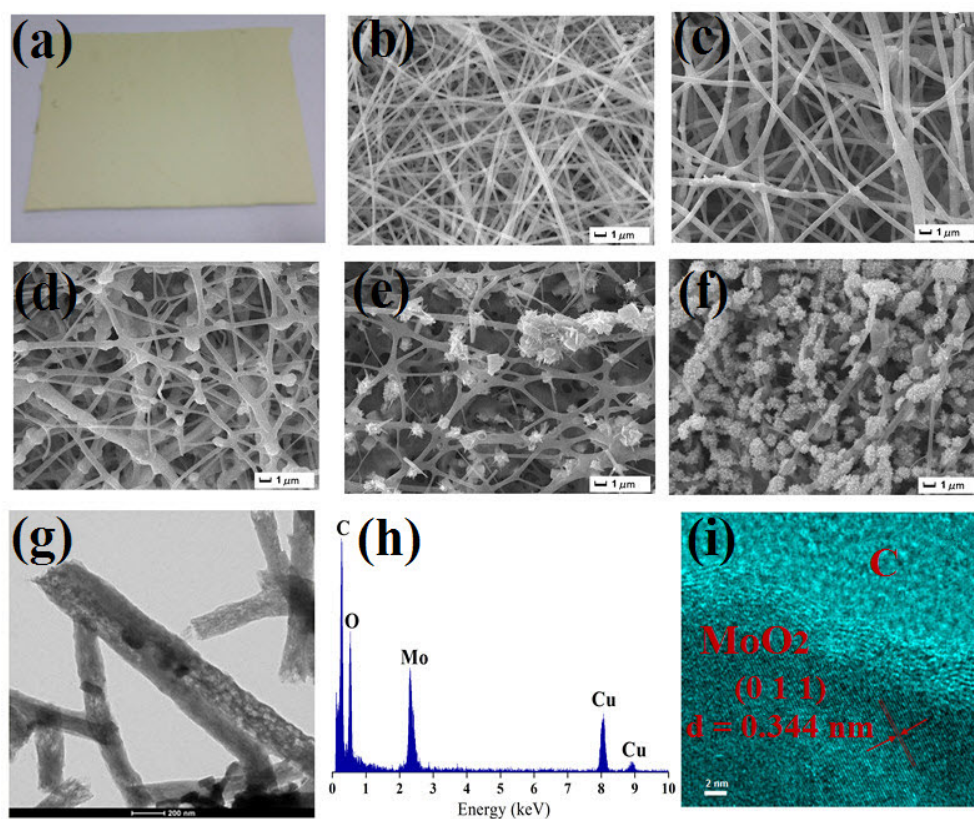


Figure 3: (a) A photo of nonwoven PAN/PMA fabric. SEM images of (b) as-prepared PAN/PMA composite fibers, (c–f) fibers calcined at 550 °C, 650 °C, 750 °C and 850 °C. (g) TEM image of MoO_2 -CNF calcined at 850 °C. (h) EDX elemental line analysis and (i) HRTEM image of MoO_2 -CNFs.

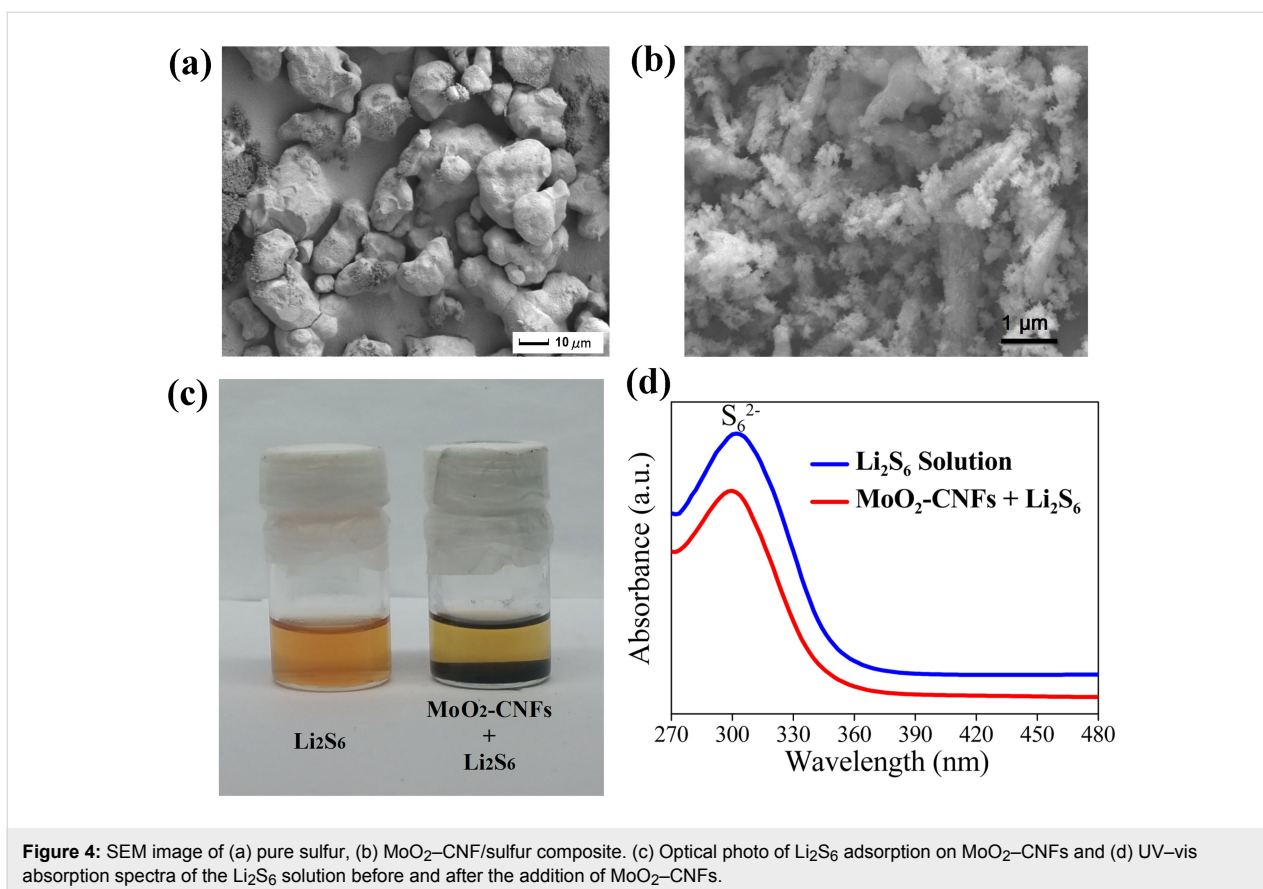


Figure 4: SEM image of (a) pure sulfur, (b) MoO₂-CNF/sulfur composite. (c) Optical photo of Li₂S₆ adsorption on MoO₂-CNFs and (d) UV-vis absorption spectra of the Li₂S₆ solution before and after the addition of MoO₂-CNFs.

was drastically changed from smooth to rough agglomerated particles upon the addition of MoO₂-CNFs. The MoO₂-CNFs acted as a conductive matrix and facilitated the dispersion of sulfur with smaller particle size, which could favor ion diffusivity in the cathode due to the reduction in the Li-ion pathways. To further evaluate the interaction between MoO₂-CNFs and polysulfides, the as-prepared MoO₂-CNFs were added into Li₂S₆ solution. In the optical photo of Figure 3c, the original yellow-brown solution turned lighter, indicating a strong adsorption. Meanwhile, UV-visible absorption spectroscopy was used to analyze the change in concentration of Li₂S₆ before and after the addition of MoO₂-CNFs. The polysulfide solution showed a broad absorption region between 270 and 330 nm, with characteristic peaks located at approximately 300 nm, ascribed to S₆²⁻ species [30]. After absorption for 0.5 h, a large decrease in the absorption peak intensity of the solution with MoO₂-CNFs at 300 nm was identified, which confirmed the improved absorption capability of the composite fibers for polysulfides.

Electrochemical performance of S/MoO₂-CNF electrodes

The electrochemical performance of cells with S/MoO₂-CNF-based electrodes were evaluated by cyclic voltammetry (CV),

galvanostatic charge-discharge and electrochemical impedance spectroscopy (EIS).

The electrochemical characteristics of the cells with S/MoO₂-CNF cathodes and pure sulfur cathodes were examined by CV in the voltage range of 1.7–3.0 V at the scanning rate of 0.1 mV s⁻¹, as shown in Figure 5a. Among these samples, all the CV curves appeared in the range of 1.93–2.05 V, 2.15–2.28 V and 2.41–2.52 V, which are typical redox reactions of Li-S batteries [31,32]. Meanwhile, the CV data confirm that the MoO₂-CNF additive is not electrochemically active in the selected voltage region. Additionally, when comparing the CV of the pure sulfur electrode, a distinguishable positive shift in the reduction-oxidation peaks of the sulfur/MoO₂-CNF composites can be observed, which confirms a relatively low potential polarization with MoO₂-CNF additives. An interesting point to note is that the highest current density of the S/MoO₂-CNF cathodes with MoO₂-CNF calcined at 850 °C indicates enhanced reaction kinetics in the charge-discharge process. Furthermore, from Supporting Information File 1, Figure S1, the coin cell of sulfur/MoO₂-CNF (850 °C) also showed the lowest voltage hysteresis (ΔV) among the cells, suggesting a highly facile electrochemical redox reaction and low resistance [33]. These findings demonstrated that

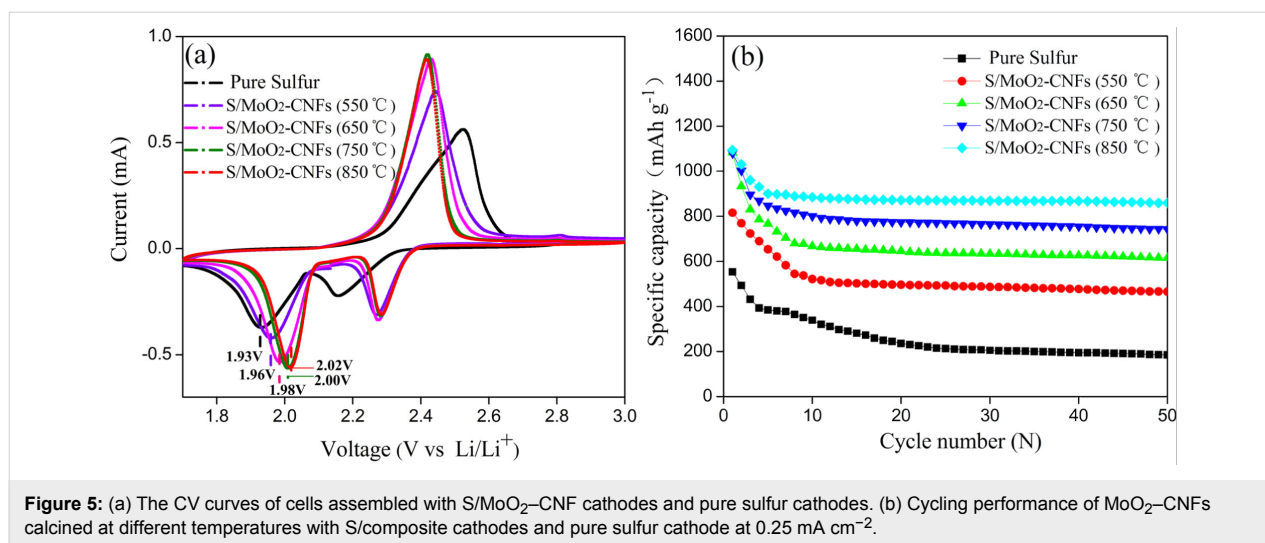


Figure 5: (a) The CV curves of cells assembled with S/MoO₂-CNF cathodes and pure sulfur cathodes. (b) Cycling performance of MoO₂-CNFs calcined at different temperatures with S/composite cathodes and pure sulfur cathode at 0.25 mA cm⁻².

MoO₂-CNFs improve the electrochemical reaction kinetics during the charge–discharge process.

Figure 5b presents the cycling performance of the cells assembled from sulfur cathodes with and without MoO₂-CNFs calcined at different temperatures. The cell assembled with the pure sulfur electrode revealed lower initial discharge capacity. After a few cycles, the discharge capacity reduced from 554 mAh g⁻¹ to 186 mAh g⁻¹. Compared to the pure sulfur cathode, the cathode performance clearly improved when MoO₂-CNFs were present in the sulfur matrix. The initial discharge capacity of the S/MoO₂-CNF cathodes with MoO₂-CNFs calcined at 550, 650, 750, and 850 °C were recorded as 816, 1082, 1079, and 1095 mAh g⁻¹, respectively. The improved performance with the addition of MoO₂-CNFs could be attributed to the polysulfide adsorption and improved electrochemical reaction kinetics of MoO₂, demonstrated by the initial specific capacity and CV curves. Meanwhile, the S/MoO₂-CNFs (calcined at 850 °C) retained the highest capacity of 860 mAh g⁻¹ after 50 cycles. The performance of the MoO₂-CNF matrix for application in Li–S batteries is also compared with several other carbon nanofibers and metal oxides fibers (Table 3), which further demonstrates the long-life behavior of the sulfur/MoO₂-CNF cathode.

The EIS technique was used to investigate the effect of the MoO₂-CNF matrix material calcined at different temperatures on the electrochemical performance of the sulfur cathode. Compared to the CV technique, the diffusion coefficients under equilibrium conditions can be expressed by electrochemical impedance spectroscopy (EIS). Additionally, the charge-transfer reaction and lithium ion diffusion in the interface of solid electrodes can be derived [38,39]. Figure 6a displays the Nyquist plots of pure sulfur and S/MoO₂-CNFs electrodes.

Table 3: Performance comparison of MoO₂-CNFs with other matrices for application in Li–S batteries.

Matrix	Cycle performance	Ref.
MoO ₂ -CNFs	860 mAh g ⁻¹ 0.25 mA cm ⁻² (≈0.1 C) per 50 cycles	this work
CNFs	207 mAh g ⁻¹ 0.1 C per 50 cycles	[34]
CNFs	390 mAh g ⁻¹ 0.1 C per 100 cycles	[35]
VGCFs	335 mAh g ⁻¹ 0.1 C per 40 cycles	[36]
CNFs	560 mAh g ⁻¹ 0.1 C per 50 cycles	[37]
Mg _{0.6} Ni _{0.4} O fibers	435 mA g ⁻¹ 0.1 C per 20 cycles	[12]

Each Nyquist plot consists of a semicircle in the high to medium frequency region and a sloping line in the low frequency region. The equivalent circuits compatible with the Nyquist diagrams are represented in the inset of Figure 6a, which contain the solution resistance (R_s), the charge-transfer resistance of the electrode (R_{ct}) and a constant phase element corresponding to the double-layer capacitance (CPE). A steep sloping line in the low-frequency region, corresponding to the Warburg impedance, was represented by W_0 . The fitting results are listed in Table 4. Obviously, the S/MoO₂-CNF cathodes possessed lower charge transfer resistance than pure sulfur cathodes, indicating better charge transfer between the sulfur and MoO₂-CNF materials. This suggested sufficient contact among sulfur and MoO₂-CNFs, which lowered the resistance for the electron transfer across the interface between both. For further confirmation, the lithium ion diffusion coefficient was calculated using Equation 2 [40,41]:

$$D_{Li} = \frac{R^2 T^2}{2A^2 n^4 F^4 C^2 \sigma^2}, \quad (2)$$

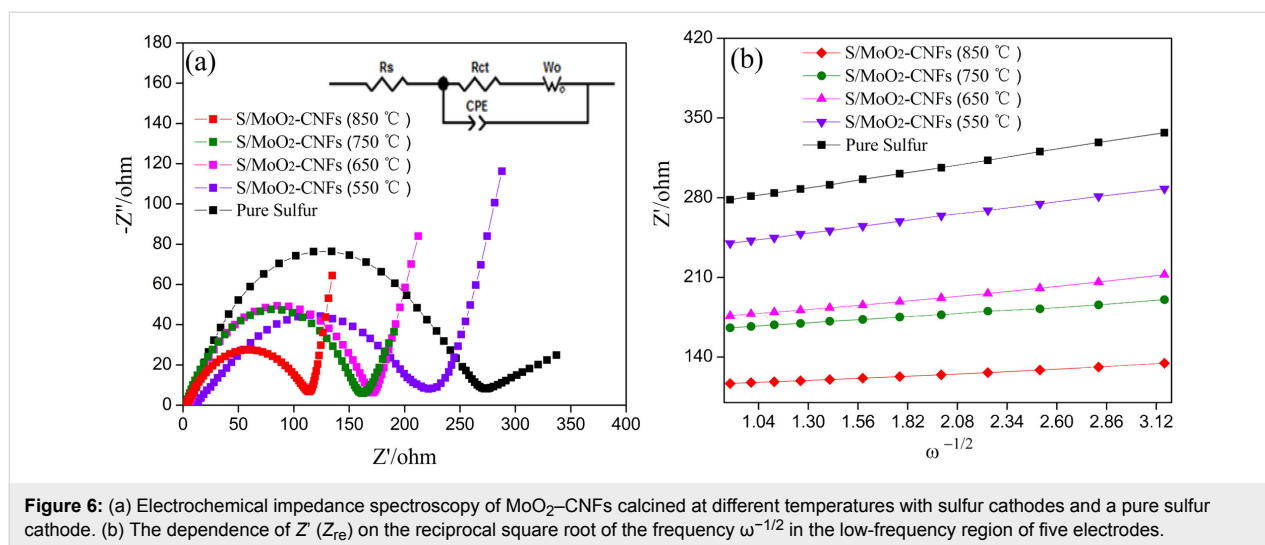


Figure 6: (a) Electrochemical impedance spectroscopy of MoO₂-CNFs calcined at different temperatures with sulfur cathodes and a pure sulfur cathode. (b) The dependence of Z' (Z_{re}) on the reciprocal square root of the frequency $\omega^{-1/2}$ in the low-frequency region of five electrodes.

Table 4: Impedance parameters of the electrodes.

Electrodes	R_s (Ω)	R_{ct} (Ω)	D_{Li} ($\text{cm}^2 \text{s}^{-1}$)
sulfur/MoO ₂ -CNF (850 °C)	1.387	113.92	8.42×10^{-14}
sulfur/MoO ₂ -CNF (750 °C)	1.584	161.15	4.38×10^{-14}
sulfur/MoO ₂ -CNF (650 °C)	2.614	169.53	2.05×10^{-14}
sulfur/MoO ₂ -CNF (550 °C)	3.004	221.59	1.16×10^{-14}
pPure sulfur	3.052	274.34	7.71×10^{-15}

where D_{Li} represents the diffusion coefficient of the lithium ion, R is the gas constant, T is the absolute temperature, A is the surface area of electrode, n is the number of electrons per molecule during the reaction, F is the Faraday constant, C is the concentration of lithium ions, and σ is the Warburg factor calculated through Equation 3 [40,41],

$$Z_{re} = R_s + R_{ct} + \varphi \omega^{-1/2}, \quad (3)$$

where φ is the slope of the plots and Z_{re} is the reciprocal root square at the lower angular frequencies ($\omega^{-1/2}$), presented in Figure 6b.

Conclusion

MoO₂-CNF materials were prepared using the electrospinning process of PAN/PMA mixtures, followed by calcination treatments. XRD, FTIR and Raman results suggest that MoO₂-CNFs were obtained after being calcined at 550 °C and complete removal of the inorganic compound. The SEM images showed that the as-prepared MoO₂-CNF composite fibers had a smooth surface which turned to rough after calcination, revealing the increased crystallinity of MoO₂ associated with the rise of the calcination temperature. The obtained MoO₂-CNFs were

applied to a sulfur matrix for Li-S batteries and shown to exhibit high capacity when compared to electrodes with pure sulfur. The improved electrochemical performance could be attributed to the adsorption of polysulfide and acceleration of the electrochemical reaction kinetics during the charge-discharge process. The EIS results demonstrated that S//MoO₂-CNF composites display a markedly higher lithium-ion diffusion coefficient, a low interfacial resistance and much better electrochemical performance than the pristine sulfur cathode. The proposed electrospinning technique might open new avenues for making promising nanofibers for practical applications.

Experimental

Synthesis of MoO₂-CNFs

Phosphomolybdic acid (PMA: H₃PO₄·12MoO₃), polyacrylonitrile (PAN, $M_w = 150,000$) and *N,N*-dimethylformamide (DMF) were purchased from Sinopharm Chemical Reagent Co., Ltd. All the reagents were used as-received without further purification.

In a typical procedure, a PAN solution (10 wt %) was prepared by dissolving PAN powder in DMF and stirring for 12 h. Next, PMA (3 g) was added to the above solution and vigorously stirred for 24 h at room temperature to form a sol-gel solution for further electrospinning. The solution was then loaded into 10 mL plastic syringes equipped with a 9-gauge stainless steel needle. A high voltage power supply was used to provide a voltage of 15 kV to the needle tips and the rotating drum collector covered by aluminum foil served as the counter electrode. The distance between the needle tips and drum collector was set to 18 cm and the flow rate of the solution to 0.5 mL h⁻¹. The as-prepared electrospun nanofibers were preoxidized at 260 °C for 2 h in air and calcined at different temperatures for 4 h under argon atmosphere. Scheme S1 in Supporting

Information File 1 illustrates the procedure used for preparing MoO₂-CNFs.

Preparation of S/MoO₂-CNF electrodes

Sulfur/MoO₂-CNF (S/MoO₂-CNF) composites were prepared by mixing sulfur and MoO₂-CNFs in a mortar at the weight ratio of 1:1. The resulting S/MoO₂-CNF composites were gradually dried in air for 6 h then heated to 155 °C for 6 h in a sealed 25 mL teflon-lined stainless-steel autoclave. After cooling down to room temperature, S/MoO₂-CNF composites were obtained. Next, the as-prepared S/MoO₂-CNF composites were mixed with acetylene black and polyvinylidene fluoride (PVDF) in *N*-methyl-2-pyrrolidone (NMP) at a weight ratio of 7:2:1. The slurry was spread onto aluminum foil (thickness: 20 μm) and dried in vacuum at 60 °C for 12 h. Electrodes were made from punching circular discs with a diameter of 12 mm and sulfur loadings of 1.5 mg cm⁻² were applied. The thickness of the electrodes was 35 μm. For comparison, a pure sulfur cathode was prepared using the same procedure by mixing sulfur, acetylene black and PVDF at the weight ratio of 7:2:1. The S/MoO₂-CNF electrode is schematically displayed in Scheme S2 of Supporting Information File 1.

Materials characterization

The crystalline phases of the samples were determined by X-ray diffraction (XRD, Rigaku D/Mmax 2500PC) using Cu K α radiation ($\lambda = 1.5406 \text{ \AA}$). The average grain size (D) of the MoO₂ nanoparticles was calculated using the Scherrer equation ($D = 0.89\lambda/(\beta\cos\theta)$), where λ represents the wavelength of the X-ray diffraction, β is the full width at half maximum of the relevant diffraction peak, and θ is the diffraction angle. The Raman spectra were recorded on an American Thermo-Fisher spectrometer using an Ar⁺ laser at 532 nm. The Brunauer–Emmett–Teller (BET) surface area was determined by nitrogen adsorption–desorption using a NOVA 2000e analyzer. The presence of functional groups was examined by Fourier transform infrared spectrometry (FTIR, Avatar-370 spectrometer) using the standard method of KBr in the scanning range of 400–4000 cm⁻¹. The size and morphology of the fibers was determined by scanning electron microscopy (SEM, JSM-7001F). Details concerning the morphology and structure were examined by high-resolution transmission electron microscopy (HRTEM, Tecnai G2 F30), operated at an accelerating voltage of 200 kV. Selected specimens were examined with energy dispersive X-ray (EDX) spectroscopy and elemental mapping attached to the HRTEM operating at 200 kV.

The adsorption ability was determined by preparing a Li₂S₆ solution through the addition of Li₂S to sulfur at the molar ratio of 1:5 in tetrahydrofuran (THF) under stirring. The obtained solution containing about 1.8 mg mL⁻¹ Li₂S₆ was used for the

sulfide adsorption test. MoO₂-CNFs were added to 10.0 mL of Li₂S₆/TFH solution and the mixture was adequately stirred for 0.5 h. The ability of the MoO₂-CNF composite to adsorb Li₂S₆ was evaluated by UV–vis spectroscopy (UV-1800PC, Shanghai Mapada Instrument Co. Ltd).

Electrochemical measurements

The electrochemical performance of the samples was measured in CR 2032-type coin cells. The electrolyte contained 1 M lithium bis(trifluoromethanesulfone)imide (LITFSI) and 0.1 M LiNO₃ dissolved in 1,3-dioxolane (DOL) and 1,2-dimethoxyethane (DME) at a volume ratio of 1:1. The electrolyte solution volume used in the cells was 75 μL. The coin cells were galvanostatically charged–discharged at 0.25 mA/cm² (1 C = 1675 mA g⁻¹) and a voltage ranging from 1.7 and to 3.0 V (vs Li/Li⁺) using a CT2001A cell test instrument (LAND model, Wuhan RAMBO testing equipment, Co. Ltd.). The CV and EIS measurements were conducted on a VMP2 electrochemical workstation (DHS Instruments Co. Ltd.). The CV curves were recorded at a scan rate of 0.1 mV s⁻¹ in the voltage range of 1.7–3.0 V. The EIS spectra were measured in the frequency range of 0.1–100 kHz with a disturbance amplitude of 10 mV.

Supporting Information

Supporting Information File 1

Additional experimental data and experimental schemes.
[<https://www.beilstein-journals.org/bjnano/content/supplementary/2190-4286-9-28-S1.pdf>]

Acknowledgements

This work was financially supported by the National Natural Science Foundation of China (Grant No. 51504101, 51474113), the Natural Science Foundation of Jiangsu Province (Grant No. BK20150514), the China Postdoctoral Science Foundation (Grant No. 2017M621640), the Natural Science Foundation of Jiangsu Provincial Higher Education of China (Grant No. 15KJB430006), the Start-up Foundation of Jiangsu University for Senior Talents (Grant No. 15JDG014).

References

- Fotouhi, A.; Auger, D. J.; Propp, K.; Longo, S.; Wild, M. *Renewable Sustainable Energy Rev.* **2016**, *56*, 1008–1021. doi:10.1016/j.rser.2015.12.009
- Hua, W.; Yang, Z.; Nie, H.; Li, Z.; Yang, J.; Guo, Z.; Ruan, C.; Chen, X.; Huang, S. *ACS Nano* **2017**, *11*, 2209–2218. doi:10.1021/acsnano.6b08627
- Juhl, A. C.; Schneider, A.; Ufer, B.; Brezesinski, T.; Janek, J.; Fröba, M. *Beilstein J. Nanotechnol.* **2016**, *7*, 1229–1240. doi:10.3762/bjnano.7.114

4. Wu, X.; Yao, S.; Hou, J.; Jing, M.; Qian, X.; Shen, X.; Xiang, J.; Xi, X. *J. Nanosci. Nanotechnol.* **2017**, *17*, 2482–2487. doi:10.1166/jnn.2017.13907
5. Zhong, J.; Wang, S.; Sha, Y.; Liu, M.; Cai, R.; Li, L.; Shao, Z. *J. Mater. Chem. A* **2016**, *4*, 9526–9535. doi:10.1039/C6TA03187K
6. Zhao, W.; Yu, Y.; Chen, H.; DiSalvo, F. J.; Abruña, H. D. *J. Am. Chem. Soc.* **2013**, *135*, 16736–16743. doi:10.1021/ja409508q
7. Evers, S.; Nazar, L. F. *Acc. Chem. Res.* **2013**, *46*, 1135–1143. doi:10.1021/ar3001348
8. Luan, K.; Yao, S.; Zhang, Y.; Zhuang, R.; Xiang, J.; Shen, X.; Li, T.; Xiao, K.; Qin, S. *Electrochim. Acta* **2017**, *252*, 461–469. doi:10.1016/j.electacta.2017.09.028
9. Xue, M.; Zhou, Y.; Geng, J.; Zeng, P.; Xu, Y.; Wang, Y.; Tang, W.; Wu, P.; Wei, S.; Zhou, Y. *RSC Adv.* **2016**, *6*, 91179–91184. doi:10.1039/C6RA19573C
10. Wei, S. Z.; Li, W.; Cha, J. J.; Zheng, G.; Yang, Y.; McDowell, M. T.; Hsu, P.-C.; Cui, Y. *Nat. Commun.* **2013**, *4*, 1331. doi:10.1038/ncomms2327
11. Li, Z.; Zhang, J.; Lou, X. W. *Angew. Chem., Int. Ed.* **2015**, *54*, 12886–12890. doi:10.1002/anie.201506972
12. Tang, H.; Yao, S.; Jing, M.; Wu, X.; Hou, J.; Qian, X.; Rao, D.; Shen, X.; Xi, X.; Xiao, K. *J. Alloys Compd.* **2015**, *650*, 351–356. doi:10.1016/j.jallcom.2015.07.264
13. Seh, Z. W.; Yu, J. H.; Li, W.; Hsu, P.-C.; Wang, H.; Sun, Y.; Yao, H.; Zhang, Q.; Cui, Y. *Nat. Commun.* **2014**, *5*, 5017. doi:10.1038/ncomms6017
14. Yuan, Z.; Peng, H.-J.; Hou, T.-Z.; Huang, J.-Q.; Cheng, C.-M.; Wang, D.-W.; Cheng, X.-B.; Wei, F.; Zhang, Q. *Nano Lett.* **2016**, *16*, 519–527. doi:10.1021/acs.nanolett.5b04166
15. Zhang, S. S.; Tran, D. T. *J. Mater. Chem. A* **2016**, *4*, 4371–4374. doi:10.1039/C6TA01214K
16. Yao, S.; Xue, S.; Zhang, Y.; Shen, X.; Qian, X.; Li, T.; Xiao, K.; Qin, S.; Xiang, J. *J. Mater. Sci.: Mater. Electron.* **2017**, *28*, 7264–7270. doi:10.1007/s10854-017-6410-z
17. Pang, Q.; Kundu, D.; Cuisinier, M.; Nazar, L. F. *Nat. Commun.* **2014**, *5*, 4759. doi:10.1038/ncomms5759
18. Pang, Q.; Kundu, D.; Nazar, L. F. *Mater. Horiz.* **2016**, *3*, 130–136. doi:10.1039/C5MH00246J
19. Hu, B.; Mai, L.; Chen, W.; Yang, F. *ACS Nano* **2009**, *3*, 478–482. doi:10.1021/nn800844h
20. Lu, Y.; Ang, H.; Yan, Q.; Fong, E. *Chem. Mater.* **2016**, *28*, 5743–5752. doi:10.1021/acs.chemmater.6b01966
21. Li, X.-y.; Xiao, Q.-g.; Gao, Y.-y.; Zhang, H.-l.; Xu, H.-b.; Zhang, Y. *J. Alloys Compd.* **2017**, *723*, 1113–1120. doi:10.1016/j.jallcom.2017.06.274
22. Yang, L. C.; Sun, W.; Zhong, Z. W.; Liu, J. W.; Gao, Q. S.; Hu, R. Z.; Zhu, M. *J. Power Sources* **2016**, *306*, 78–84. doi:10.1016/j.jpowsour.2015.11.073
23. Yang, L.; Li, X.; Quyang, Y.; Gao, Q.; Quyang, L.; Hu, R.; Liu, J.; Zhu, M. *ACS Appl. Mater. Interfaces* **2016**, *8*, 19987–19993. doi:10.1021/acsami.6b05049
24. Zhang, C.-L.; Yu, S.-H. *Mater. Horiz.* **2016**, *3*, 266–269. doi:10.1039/C6MH00045B
25. Liu, M.; Xie, W.; Gu, L.; Qin, T.; Hou, X.; He, D. *Beilstein J. Nanotechnol.* **2016**, *7*, 1289–1295. doi:10.3762/bjnano.7.120
26. Zhang, J.; Cai, Y.; Hou, X.; Song, X.; Lv, P.; Zhou, H.; Wei, Q. *Beilstein J. Nanotechnol.* **2017**, *8*, 1297–1306. doi:10.3762/bjnano.8.131
27. Li, H.; Hong, W.; Cui, Y.; Fan, S.; Zhu, L. *J. Alloys Compd.* **2013**, *569*, 45–51. doi:10.1016/j.jallcom.2013.03.165
28. Naouel, R.; Touati, F.; Gharbi, N. *Solid State Sci.* **2010**, *12*, 1098–1102. doi:10.1016/j.solidstatesciences.2010.04.015
29. Dharmaraj, N.; Park, H. C.; Lee, B. M.; Viswanathamurthi, P.; Kim, H. Y.; Lee, D. R. *Inorg. Chem. Commun.* **2004**, *7*, 431–433. doi:10.1016/j.inoche.2003.12.033
30. Han, K.; Shen, J.; Hao, S.; Ye, H.; Wolverton, C.; Kung, M. C.; Kung, H. H. *ChemSusChem* **2014**, *7*, 2545–2553. doi:10.1002/cssc.201402329
31. Han, S.-C.; Song, M.-S.; Lee, H.; Kim, H.-S.; Ahn, H.-J.; Lee, J.-Y. *J. Electrochem. Soc.* **2003**, *150*, A889–A893. doi:10.1149/1.1576766
32. Babu, G.; Ababtain, K.; Simon, N. K. Y.; Arava, L. M. R. *Sci. Rep.* **2015**, *5*, 8763. doi:10.1038/srep08763
33. Cui, Z.; Zu, C.; Zhou, W.; Manthirama, A.; Goodenough, J. B. *Adv. Mater.* **2016**, *28*, 6926–6931. doi:10.1002/adma.201601382
34. Lu, S.; Cheng, Y.; Wu, X.; Liu, J. *Nano Lett.* **2013**, *13*, 2485–2489. doi:10.1021/nl400543y
35. Yang, X.; Zhu, W.; Cao, G.; Zhao, X. *RSC Adv.* **2016**, *6*, 7159–7171. doi:10.1039/C5RA24129D
36. Wu, Y.; Gao, M.; Li, X.; Liu, Y.; Pan, H. *J. Alloys Compd.* **2014**, *608*, 220–228. doi:10.1016/j.jallcom.2014.04.073
37. Rao, M. M.; Geng, X. Y.; Li, X. P.; Hu, S. J.; Li, W. S. *J. Power Sources* **2012**, *212*, 179–185. doi:10.1016/j.jpowsour.2012.03.111
38. Huang, X.; Li, X.; Wang, H.; Pan, Z.; Qu, M.; Yu, Z. *Electrochim. Acta* **2010**, *55*, 7362–7366. doi:10.1016/j.electacta.2010.07.036
39. Cañas, N. A.; Hirose, K.; Pascucci, B.; Wagner, N.; Friedrich, K. A.; Hiesgen, R. *Electrochim. Acta* **2013**, *97*, 42–51. doi:10.1016/j.electacta.2013.02.101
40. Shenouda, A. F.; Liu, H. K. *J. Electrochem. Soc.* **2010**, *157*, A1183–A1187. doi:10.1149/1.3479425
41. Bard, A. J.; Faulkner, L. R., Eds. *Electrochemical Methods: Fundamentals and Applications*, 2nd ed.; John Wiley & Sons, Inc.: New York, NY, U.S.A., 2001.
42. Fan, C.-Y.; Xiao, P.; Li, H.-H.; Wang, H.-F.; Zhang, L.-L.; Sun, H.-Z.; Wu, X.-L.; Xie, H.-M.; Zhang, J.-P. *ACS Appl. Mater. Interfaces* **2015**, *7*, 27959–27967. doi:10.1021/acsami.5b10300

License and Terms

This is an Open Access article under the terms of the Creative Commons Attribution License (<http://creativecommons.org/licenses/by/4.0>), which permits unrestricted use, distribution, and reproduction in any medium, provided the original work is properly cited.

The license is subject to the *Beilstein Journal of Nanotechnology* terms and conditions: (<https://www.beilstein-journals.org/bjnano>)

The definitive version of this article is the electronic one which can be found at: doi:10.3762/bjnano.9.28